Chapter 1

Experimental Background

The subject of this series of lectures is the analysis of data generated by a dynamical system operating in a chaotic regime. More specifically, we describe how to extract, from chaotic data, topological signatures that determine the stretching and squeezing mechanisms which act on flows in phase space and which are responsible for generating chaotic data.

In the first section of this introductory chapter we describe, for purposes of motivation, a laser that has been operated under conditions in which it behaved chaotically. The topological methods of analysis that we describe in this lecture series were developed in response to the challenge of analyzing chaotic data sets generated by this laser.

In the second section we list a number of questions which we would like to be able to answer when analyzing a chaotic signal. None of these questions can be addressed by the older tools for analyzing chaotic data: estimates of the spectrum of Lyapunov exponents and estimates of the spectrum of fractal dimensions. The question that we would particularly like to be able to answer is this: How does one model the dynamics? To answer this question we must determine the stretching and squeezing mechanisms that operate together— repeatedly—to generate chaotic data. The stretching mechanism is responsible for *sensitivity to initial conditions* while the squeezing mechanism is responsible for *recurrent nonperiodic behavior*. These two mechanisms operate repeatedly to generate a strange attractor with a self-similar structure.

A new analysis method, topological analysis, has been developed to respond to the fundamental question just stated. At the present time this method is suitable only for strange attractors that can be embedded in three-dimensional spaces. However, for such strange attractors it offers a complete and satisfying resolution to this question. The results are previewed in the third section of this chapter.

It is astonishing that the topological analysis tools that we describe have provided answers to more questions than we asked originally. This analysis procedure has also raised more questions than we have answered. We hope that the interaction between experiment and theory and between old questions

answered and new questions raised will hasten evolution of the field of nonlinear dynamics.

1.1   Laser with Modulated Losses

The possibility of observing chaos in lasers was originally demonstrated by and by Gioggia and Abraham. The use of lasers as a testbed for generating deterministic chaotic signals has two major advantages over fluid and chemical systems, which until that time had been the principal sources for chaotic data:

1. The time scales intrinsic to a laser (10^{-7} to 10^{-3} s) are much shorter than the time scales in fluid experiments and oscillating chemical reactions. This is important for experimentalists, since it is possible to explore a very large parameter range during a relatively short time.

2. Reliable laser models exist in terms of a small number of ordinary differential equations whose solutions show close qualitative similarity to the behavior of the lasers that are modeled.

The topological methods described in the remainder of this work were originally developed to understand the data generated by a laser with modulated losses. A schematic of this laser is shown in Fig. 1.1. A CO_2 gas tube is placed between two infrared mirrors (M). The ends of the tube are terminated by Brewster angle windows, which polarize the field amplitude in the vertical direction. Under normal operating conditions, the laser is very stable. A Kerr cell (K) is placed inside the laser cavity. The Kerr cell modifies the polarization state of the electromagnetic field. This modification, coupled with the polarization introduced by the Brewster windows, allows one to change the intracavity losses. The Kerr cell is modulated at a frequency determined by the operating conditions of the laser. When the modulation is small, the losses within the cavity are small, and the laser output tracks the input from the signal generator. The input signal (from the signal generator) and the output signal (the measured laser intensity) are both recorded in a computer (C). When the modulation crosses a threshold, the laser output can no longer track the signal input. At first every other output peak has the same height, then every fourth peak, then every eighth peak, and so on.

In Fig. 1.2 we present some of the recorded and processed signals from this part of the period-doubling cascade and beyond. The signals were recorded under different operating conditions and are displayed in five lines, as follows: (a) period 1; (b) period 2; (c) period 4; (d) period 8; (e) chaos. Each of the four columns presents a different representation of the data. In the first column the intensity output is displayed as a function of time. In this presentation the period-1 and period-2 behaviors are clear but the higher-period behavior is not.

The second column displays a projection of the dynamics into a two-dimensional space, the dI/dt vs. $I(t)$ plane. In this projection, periodic orbits appear as
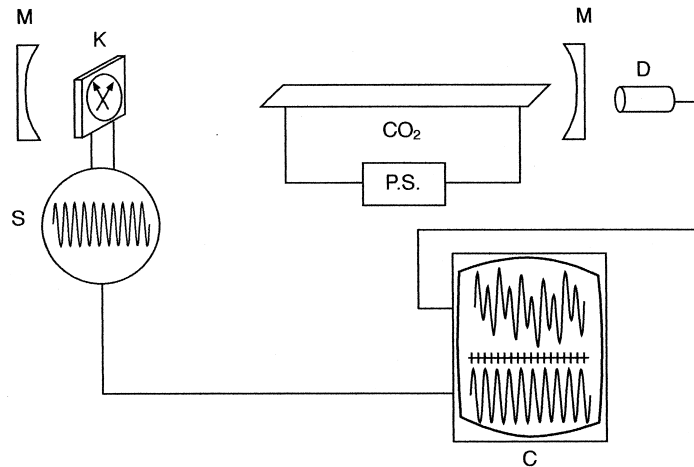
Figure 1.1: This schematic representation of a laser with modulated losses shows the carbon dioxide tube (CO_2); power source (P.S.); mirrors (M); Kerr cell (K); signal generator (S); detector (D); and computer, oscilloscope, and recorder (C). A variable electric field across the Kerr cell rotates its polarization direction and modulates the electric field amplitude within the cavity.

closed loops (deformed circles) which go around once, twice, four times, ... before closing. In this presentation the behavior of periods 1, 2, and 4 is clear. Period 8 and chaotic behavior is less clear. The third column displays the power spectrum. Not only is the periodic behavior clear from this display, but the relative intensity of the various harmonics is also evident. Chaotic behavior is manifest in the broadband power spectrum. Finally, the last column displays a stroboscopic sampling of the output. In this sampling technique, the output intensity is recorded each time the input signal reaches a maximum (or some fixed phase with respect to the maximum). There is one sample per cycle. In period-1 behavior, all samples have the same value. In period-2 behavior, every other sample has the same value. The stroboscopic display clearly distinguishes between periods 1, 2, 4, and 8. It also distinguishes periodic behavior from chaotic behavior. The stroboscopic sampling technique is equivalent to the construction of a Poincaré section for this periodically driven dynamical system. All four of these display modalities are available in real time, during the experiment.

The laser with modulated losses has been studied extensively both experimentally and theoretically. The rate equations governing the laser intensity I
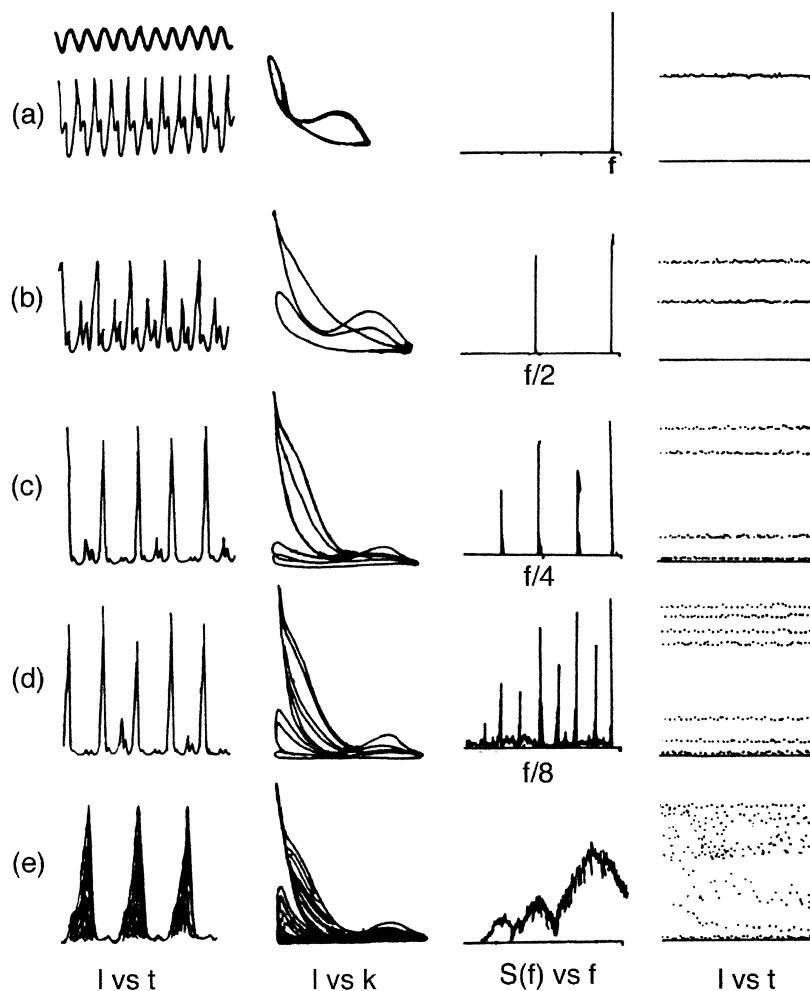
Figure 1.2: Each column provides a different representation of the experimental data. Each row describes different experimental conditions. The first column shows the recorded intensity time signal, $I(t)$. The second column presents the phase-space projection, $dI(t)/dt$ vs. $I(t)$. The third column shows the power spectrum of the recorded intensity signal. The frequencies of the Fourier components in the signal, and their relative amplitudes, jump out of this plot. The last column presents a stroboscopic plot (Poincaré section). This is a record of the intensity output at each successive peak (or more generally, at some constant phase) of the input signal. The data sets were recorded under the following experimental conditions: (a) period 1; (b) period 2; (c) period 4; (d) period 8; (e) chaotic. Reprinted with permission from Tredicce et al.

and the population inversion N are

$$\frac{dI}{dt} = -k_0 I[(1 - N) + m\cos(\omega t)]$$

$$\frac{dN}{dt} = -\gamma[(N - N_0) + (N_0 - 1)IN]$$

$$(1.1)$$

Here m and ω are the modulation amplitude and angular frequency, respectively, of the signal to the Kerr cell; N_0 is the pump parameter, normalized to $N_0 = 1$ at the threshold for laser activity; and k_0 and γ are loss rates. In dimensionless, scaled form this equation is

$$\frac{du}{d\tau} = [z - A\cos(\Omega\tau)]u$$

$$\frac{dz}{d\tau} = (1 - \epsilon_1 z) - (1 + \epsilon_2 z)u$$

$$(1.2)$$

The scaled variables are $u = I$, $z = k_0\kappa(N - 1)$, $t = \kappa\tau$, $A = k_0 m$, $\epsilon_1 = 1/\kappa k_0$, and $\kappa^2 = 1/\gamma k_0(N_0 - 1)$. The bifurcation behavior exhibited by the simple models (1.1) and (1.2) is qualitatively, if not quantitatively, in agreement with the experimentally observed behavior of this laser.

A bifurcation diagram for the laser model (1.2) is shown in Fig. 1.3. The bifurcation diagram is constructed by varying the modulation amplitude A and keeping all other parameters fixed. The overall structures of the bifurcation diagrams are similar to experimentally observed bifurcation diagrams.

This figure shows that a period-1 solution exists above the laser threshold $(N_0 > 1)$ for $A = 0$ and remains stable as A is increased until $A \sim 0.8$. It becomes unstable above $A \sim 0.8$, with a stable period-2 orbit emerging from it in a period-doubling bifurcation. Contrary to what might be expected, this is not the early stage of a period-doubling cascade, for the period-2 orbit is annihilated at $A \sim 0.85$ in an inverse saddle-node bifurcation with a period-2 regular saddle. This saddle-node bifurcation destroys the basin of attraction of the period-2 orbit. Any point in that basin is dumped into the basin of a period $4 = 2 \times 2^1$ orbit, even though there are two other coexisting basins of attraction for stable orbits of periods $6 = 3 \times 2^1$ and 4 at this value of A.

Subharmonics of period n (P_n, $n \geq 2$) are created in saddle-node bifurcations at increasing values of A and I (P_2 at $A \sim 0.1$, P_3 at $A \sim 0.3$, P_4 at $A \sim 0.7$, P_5 and higher shown in the inset). All subharmonics in this series up to period $n = 11$ have been seen both experimentally and in simulations of (1.2). The evolution (*perestroika*) of each of these subharmonics follows a standard scenario as T increases:
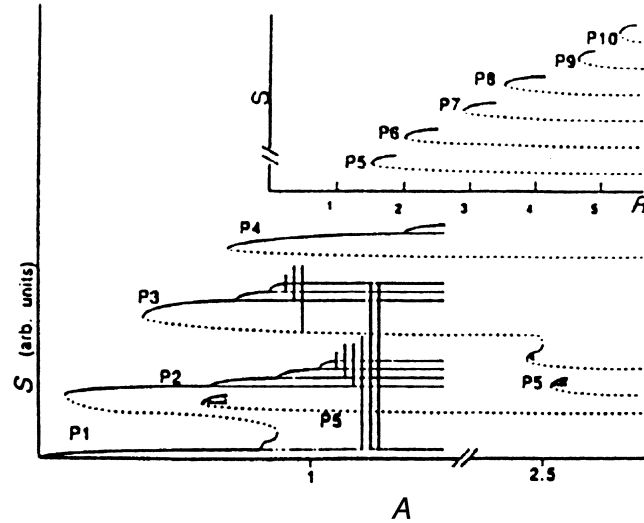
Figure 1.3: The bifurcation diagram for the laser model (1.2) is computed by varying the modulation amplitude A. Stable periodic orbits (solid lines), regular saddles (dotted lines), and strange attractors are shown. Period n branches ($P_n \geq 2$) are created in saddle-node bifurcations and evolve through the Feigenbaum period-doubling cascade as the modulation amplitude increases. There are two apparently distinct stable period-2 orbits. However, these are connected by an unstable period-2 orbit (dotted, extending from $A \simeq 0.1$ to $A \simeq 0.8$) and thus constitute a single period-2 orbit which is a *snake*. A period-3 snake is also present. Two distinct stable period-4 orbits are present and coexist over a short range of parameter values ($0.7 < A < 0.8$). The inset shows a sequence of period-n orbits (*Newhouse orbits*) for $n \geq 5$. The Smale horseshoe mechanism predicts that as many as three inequivalent pairs of period-5 orbits could exist. The locations of the two additional pairs have been shown in this diagram at $A \simeq 0.65$ and $A \simeq 2.5$. Parameter values: $\epsilon_1 = 0.03$, $\epsilon_2 = 0.009$, $\Omega = 1.5$.

1. A saddle-node bifurcation creates an unstable saddle and a node that is initially stable.

2. Each node becomes unstable and initiates a period-doubling cascade as A increases. The cascade follows the standard Feigenbaum scenario. The ratio of A intervals between successive bifurcations, and of geometric sizes of the stable nodes of periods $n \times 2^k$, have been estimated up to $k \leq 6$ for some of these subharmonics, both from experimental data and from the simulations. These ratios are compatible with the universal scaling ratios.

3. Beyond accumulation, there is a series of noisy orbits of period $n \times 2^k$ that undergo inverse period-halving bifurcations. This scenario has been predicted by Lorenz.

Additional systematic behavior has been observed. Higher subharmonics are generally created at larger values of A. They are created with smaller basins of attraction. The range of A values over which the Feigenbaum scenario is played out becomes smaller as the period n increases. In addition, the subharmonics show an ordered pattern in phase space. In Fig. 1.4 we show four stable periodic orbits that coexist under certain operating conditions. Roughly speaking, the larger period orbits exist "outside" the smaller period orbits. These orbits share many other systematics, which have been describe. In Fig. 1.5 we show an example of a chaotic time series taken for $A \sim 1.3$. The chaotic attractor based on the period-2 orbit (the period-1 orbit) has just collided with the period-3 regular saddle.

The period-doubling, accumulation, inverse noisy period-halving scenario described above is often interrupted by a crisis (Grebogi and Ott) of one type or another:

Boundary Crisis: A regular saddle on a period-n branch in the boundary of the basin of attraction surrounding either the period-n node or one of its periodic or noisy periodic progeny collides with the attractor. The basin is annihilated or enlarged.

Internal Crisis: A flip saddle of period $n \times 2^k$ in the boundary of a basin surrounding a noisy period $n \times 2^{k+1}$ orbit collides with the attractor to produce a noisy period-halving bifurcation.

External Crisis: A regular saddle of period n' in the boundary of a period n ($P_n \neq P_{n'}$) strange attractor collides with the attractor, thereby annihilating or enlarging the basin of attraction.

Figure 1.6(a) provides a schematic representation of the bifurcation diagram shown in Fig. 1.3. The different kinds of bifurcations encountered in both experiments and simulations are indicated here. These include both direct and inverse saddle-node bifurcations, period-doubling bifurcations, and boundary and external crises. As the laser operating parameters (k_0, γ, ω) change, the bifurcation diagram changes.
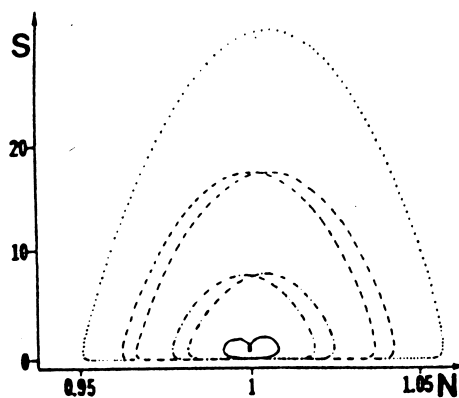
Figure 1.4: Multiple basins of attraction can coexist over a broad range of parameter values. The stable periodic orbits and the strange attractors within these basins have a characteristic organization. The coexisting orbits shown above are, from the inside to the outside: period 2 bifurcated from a period 1 branch; period 2; period 3; period 4. The two inner orbits are separated by an unstable period-2 orbit (not shown); all three are part of a snake.
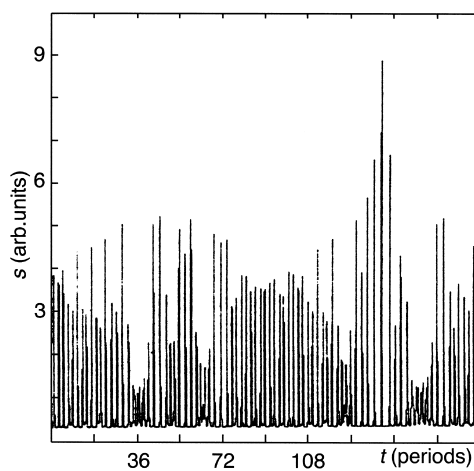
Figure 1.5: This time series from a laser with modulated losses was taken at a value of $A \sim 1.3$, which is just beyond the collision (crisis) of the strange attractors based on the period-2 and period-3 orbits. There is an alternation in this time series between noisy period-2 and noisy period-3 behavior.
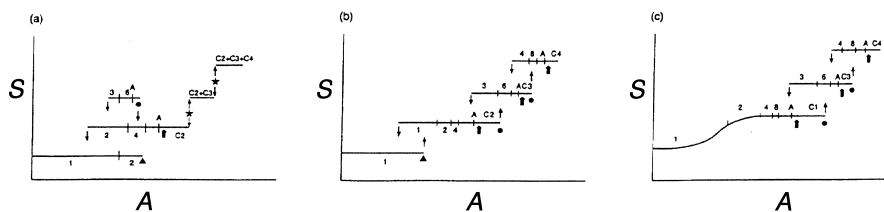
Figure 1.6: Schematics of three bifurcation diagrams for three different operating conditions of Eqs. (1.2). As control parameters change, the bifurcation diagram is modified. Slow change in control parameter values deforms the bifurcation diagram from (a) to (b) to (c). The sequence (a) to (c) shows the unfolding of the snake in the period-2 orbit. The unstable period-2 orbit connecting the two lowest branches is invisible in (a) and (b) since only stable attractors are shown. In each diagram the bifurcations are: $\downarrow$, saddle-node; $\triangle$, inverse saddle-node; , inverse saddle-node; doesn't work $\bullet$, boundary crisis; $\star$, external crisis. Period-doubling bifurcations are indicated by a small vertical line separating stable orbits of periods differing by a factor of 2. Accumulation points are indicated by A. Strange attractors based on period-n orbits are indicated by the Cn.

In Fig. 1.6(b) and (c) we show the schematics of bifurcation diagrams obtained for slightly different values of these operating—or control—parameters.

In addition to the subharmonic orbits of period n created at increasing values of A (Fig. 1.3), there are orbits of period n that do not appear to belong to that series (Newhouse series) of subharmonics. The clearest example is the period-2 orbit, which bifurcates from period 1 at $A \sim 0.8$. Another is the period-3 orbit pair created in a saddle-node bifurcation that occurs at $A \sim 2.45$. These bifurcations were seen in both experiments and simulations. It was possible to trace the unstable orbits of period 2 ($0.1 \leq A \leq 0.85$) and period 3 ($0.4 \leq A \leq 2.5$) in simulations and find that these orbits are components of an orbit snake (Alligood; Alligood, Sauer, and Yorke). This is a single orbit that folds back and forth on itself in direct and reverse saddle-node bifurcations as A increases (this is not unlike a Feynman diagram for hard scattering of an electron by a photon, which scatters the electron backward in time, creating a positron ...). The unstable period-2 orbit ($0.1 \leq T \leq 0.85$) is part of a snake. By changing operating conditions, both snakes can be eliminated [see Fig. 1.6(c)]. As a result, the "subharmonic P_2" is really nothing other than the period-2 orbit, which bifurcates from the period-1 branch P_1. Furthermore, instead of having saddle-node bifurcations creating four inequivalent period-3 orbits (at $A \sim 0.4$ and $A \sim 2.45$) there is really only one pair of period-3 orbits, the other pair being components of a snake.

Topological tools (relative rotation rates; Solari and Gilmore) were first developed to determine which orbits might be equivalent, or components of a

snake, and which are not. Components of a snake have the same topological invariants (cf. Chapter 4). These tools suggested that the Smale horseshoe mechanism was responsible for generating the nonlinear phenomena observed in both the experiments and the simulations. This mechanism predicts that additional inequivalent subharmonics of period n can exist for $n \geq 5$. Since the size of a basin of attraction decreases rapidly with n, a search was made for additional inequivalent basins of attraction of period 5. Two additional stable period-5 orbits (besides P_5) were located in simulations. Their locations are shown in Fig. 1.3 at $A \sim 0.6$ and $A \sim 2.45$. One was also located experimentally. The other may also have been seen, but its basin was too small to be certain of its existence.

Bifurcation diagrams had been observed for a variety of physical systems at that time: other lasers; electric circuits; a biological model; and a bouncing ball. Their bifurcation diagrams are similar but not identical to those shown above. This raised the question of whether similar processes were governing the description of this large variety of physical systems.

During these analyses, it became clear that the standard tools for analyzing chaotic data—estimates of the spectrum of Lyapunov exponents and estimates of the various fractal dimensions—were not sufficient for a satisfying understanding of the stretching and squeezing processes that occur in phase space and which are responsible for generating chaotic behavior. In the laser we found many coexisting basins of attraction, some containing a periodic attractor, others containing a strange attractor. The rapid alternation between periodic and chaotic behavior as control parameters (e.g., A and Ω) were changed meant that Lyapunov exponents and fractal dimensions depended on the basins and varied at least as rapidly.

For this reason we sought to develop additional tools for the analysis of data generated by dynamical systems that exhibit chaotic behavior. The objective was to develop measures that were invariant under control parameter changes.

1.2   Objectives of a New Analysis Procedure

In view of the experiments just described and the data that they generated, we hoped to develop a procedure for analyzing data that achieved a number of objectives. These included an ability to answer the following questions:

1. Is it possible to develop a procedure for understanding dynamical systems *and their evolution* (perestroikas) as the control parameters (e.g., k_0, m, γ, or A, Ω, ϵ_1, ϵ_2) change?

2. Is it possible to identify a dynamical system by means of topological invariants, following suggestions proposed by Poincaré?

3. Can selection rules be constructed under which it is possible to determine the order in which periodic orbits can be created and/or annihilated by standard bifurcations? Or when different orbits might belong to a single snake?

4. Is it possible to determine when two strange attractors are (a) equivalent in the sense that one can be transformed into the other without creating or annihilating orbits; or (b) adiabatically equivalent (one can be deformed into the other by changing parameters to create or annihilate only a small number of orbit pairs below any period); or (c) inequivalent (there is no way to transform one into the other)?

1.3   Preview of Results

A new topological analysis procedure was developed in response to the questions asked of the data initially. These questions are summarized in Section 1.2. The remarkable result is that there is now a positive and constructive answer to the question: How can I look at experimental data, such as shown in Fig. 1.2 or 1.5, and extract useful information, let alone information about stretching and squeezing, let alone a small set of integers?

This new analysis procedure answered more questions than were asked originally. It also raised a great many additional questions. This is one of the ways we know that we are on the right track.

The results of this new topological analysis procedure are presented throughout this book. Below we provide a succinct preview of the major accomplishments of this topological analysis tool.

- It is possible to classify low-dimensional strange attractors. These are strange attractors that exist in three-dimensional spaces.

- This classification is topological in nature.

- This classification exists at two levels: a macroscopic level and a microscopic level.

- It is discrete at both levels. Thus, there exists a doubly discrete classification for low-dimensional strange attractors.

- This doubly discrete classification depends in an essential way on the (unstable) periodic orbits, which are embedded in strange attractors.

- At the macro level the classification is by means of a geometric structure that describes the topological organization of *all* the unstable periodic orbits that exist in a *hyperbolic* strange attractor. This geometric structure is called variously a (two-dimensional) *branched manifold*, *knot-holder*, or *template*.

- Branched manifolds can be identified by a set of integers. Thus, at the macro level the classification is discrete.

- At the micro level the classfication is by means of a set of orbits in a *nonhyperbolic* strange attractor whose existence implies the presence of all the other orbits that can be found in the nonhyperbolic strange attractor. This subset of orbits is called a *basis set of orbits*.

- To any given period, a basis set of orbits is also discrete.

- As control parameters change, the basis set of orbits changes. The changes that are allowed are limited by topological arguments.

- Each different sequence of basis sets describing the transition from the laminar to the hyperbolic limit describes a different route to chaos. Each different route to chaos is a different path in a forcing diagram, shown in Fig. 9.8.

- During this transition the underlying branched manifold is robust: It generally does not change.

- Large changes in control parameter values can cause changes in the underlying branched manifold.

- These changes occur by adding branches to or removing branches from the branched manifold. The branch changes that are allowed are also limited by topological and continuity arguments.

- The information required for this doubly discrete classification of strange attractors can be extracted from experimental data.

- The data requirements are not heavy. Data sets of limited length are required.

- The data need not be exceptionally clean. Only a modest signal-to-noise level is required. The analysis method degrades gracefully with noise. Specifically, as the noise level degrades the data, it becomes more difficult to identify the higher-period orbits, which are the least important for this analysis. The most important orbits, those of lowest period, persist longest with increasing noise. As a result, "Murphy is on vacation" (author of the famous law).

- The data analysis method comes endowed with a rejection criterion.

- The branched manifold identifies the stretching and squeezing mechanisms that generate chaotic behavior.

- Thus, this doubly discrete classification describes "how to model the dynamics."